Eur. Phys. J. D (2015) 69: 133
DOI: 10.1140/epjd/e2015-60104-x

THE EUROPEAN PHYSICAL JOURNAL D

Regular Article

High-order harmonic generation enhanced by coherent population return

Alexis Chacón[1,2,a], Marcelo F. Ciappina[3,b], and Alvaro Peralta Conde[4]

[1] ICFO-Institut de Ciéncies Fotóniques, Mediterranean Technology Park, 08860 Castelldefels (Barcelona), Spain
[2] Grupo de Investigación en Óptica Extrema, Universidad de Salamanca, 37008 Salamanca, Spain
[3] Max-Planck-Institut für Quantenoptik, Hans-Kopfermann-Strasse 1, 85748 Garching, Germany
[4] Centro de Láseres Pulsados (CLPU), Parque Científico USAL, 37185 Villamayor, Salamanca, Spain

Received 17 February 2015 / Received in final form 16 April 2015
Published online 15 May 2015 –

Abstract. We present computations of high-order harmonic generation in atoms by using the coherent population return technique. This approach consists in two steps: firstly, the active medium is prepared in a coherent superposition of two bound states using a relatively long laser pulse which has a photon energy close to the energy gap between the states and then, the system is driven by an ultrashort infrared laser pulse. We demonstrate, by employing the numerical solution of the time-dependent Schrödinger equation in one and three dimensions, that using this scheme it is possible to enhance the harmonic conversion efficiency by several orders of magnitude. Our numerical results show that, on one hand the increase in ionization efficiency is responsible of an enhancement in the harmonic signal and on the other hand, the coherent preparation of the medium produces a much richer structure of the harmonic emission.

1 Introduction

In the last decades high-order harmonic generation (HHG) has opened new fields of research with relevant impact in several scientific disciplines. Not only the prospect to synthesize attosecond pulses from the generated harmonics has been used to access processes whose temporal dynamics was inaccessible before (see for example [1–4]), but also the possibility to use the short wavelengths generated has proven its importance in fields like femtochemistry or surface science [5–8]. Within the different approaches to describe HHG the most natural one is the so-called "three-step" or simple man's model [9,10]. In this picture, first, the laser electric field, with intensities on the order of 10^{13}–10^{14} W/cm^2, modifies the Coulomb potential of the atom in such a way that allows the electron to be ionized by tunneling. Second, once in the continuum, this electron is accelerated by the electric field gaining kinetic energy. Third, when the electric field reverses its direction, the electron comes back to the ion core and re-collides with it. This re-collision leads to the recombination process of the electron with the ground state and then, the system emits in form of harmonics of the fundamental frequency the excess of energy gained in the process [9,11].

Nowadays experimental, as well as theoretical, efforts within this field are devoted to two main tasks. The first one is devoted to extend the frequency of the generated harmonics in order to not only obtain shorter attosecond pulses, but also coherent radiation in the X-ray region. It is shown that the harmonic cutoff energy $E_{\max} = I_p + 3.17U_p$ is limited by the ionization potential I_p of the system and the ponderomotive energy $U_p = \epsilon_0^2/4\omega^2$ of the electron in the laser field (atomic units are used throughout this paper unless otherwise stated). Here, ϵ_0 and ω are the peak amplitude of the laser electric field and its carrier frequency, respectively. According to the maximum photon energy $E_{\max}$, the routes for obtaining a long harmonic cutoff rely either on increasing the laser intensity or the laser wavelength. Unfortunately both routes compromises seriously the efficiency of the HHG process. It is worth of mention recent experimental and theoretical developments which allow, on one hand, to extend the harmonic cutoff by using a combination of spatial and temporal synthesized fields [12] and complex pulse shaping techniques [13,14] and, on the other hand, to increase the harmonic yield at intensities beyond the tunnel regime taking advantage of a particular kind of laser-induced electron trajectories [15,16].

The second important issue still to be solved is the low efficiency of the HHG emission which potentially limits the possible applications of such process. Once again the

[a] e-mail: alexis.chacon@icfo.es
[b] e-mail: marcelo.ciappina@mpq.mpg.de

increment of the incident laser intensity does not work due to the depletion of the ground state, reducing therefore the harmonic emission. One of the feasible strategies to overcome this problem, besides of the ones studied in [15–17], is to prepare initially the active medium, i.e. the atom or molecule, in a coherent superposition of states. This approach has been analyzed theoretically by several authors (see e.g. [18–24]) demonstrating an enhancement in the harmonic conversion efficiency, but without taking into account a conceivable experimental scheme for the initial preparation of the medium. In addition, a combination of prepared atoms and chirped pulses was investigated in reference [25] meanwhile experimental studies using an incoherent excited medium were presented in reference [26]. Furthermore, in reference [17], Biegert et al., have experimentally observed that the HHG spectra can also be enhanced by combining an Attosecond Pulse Train (APT) and an IR laser field. In this scheme the assistance of the APT replaces the tunneling ionization process by a single-photon ionization step. In spite of the fact that application of the ATP to enhance the harmonic emission represent a plausible alternative, not all the produced harmonics are enhanced with this approach. Finally, in reference [27], high-order harmonic generation experiments probing the electronic coherence in dynamically aligned molecules were performed.

The state preparation of quantized media is usually achieved using laser-based coherent techniques. In general, the ability to control the inherent coherent nature of laser-matter interaction has proven to be a very valuable tool. For instance this control can be used to steer population distributions, generate coherent superposition of quantum states, support spectroscopical investigations, manipulate linear or nonlinear optical properties and control photofragmentation channels. Techniques like stimulated Raman adiabatic passage (STIRAP) [28], electromagnetic induced transparency (EIT) [29,30], retroreflection induced adiabatic passage (RIBAP) [31,32], or coherent population return (CPR) [33,34] have been successfully applied presenting a great robustness with respect to the experimental parameters. Amongst these techniques CPR is specially relevant for the preparation of quantum states because of its experimental simplicity. CPR allows, during the interaction time, to create a coherent superposition of states with weights controlled by the magnitude of the interaction. Recently in the group of Prof. Dr. Halfmann a modified version of CPR was successfully applied to maximize the nonlinear response of a medium by generating a maximum coherent superposition, i.e., a superposition with equal probability amplitudes, of two energetically distant quantum states. Based on this implementation, it was possible to enhance the yield of the third harmonic generation signal in Xe atoms [35].

In this paper, we propose to first prepare a medium in a coherent superposition of states using the CPR technique, and then induce the HHG emission. Using this scheme, the results of the time-dependent Schrödinger equation (TDSE) integrated in one and three dimensions clearly show not only an enhancement of at least two orders of magnitude in the harmonic emission, but also the appearance of new and distinctive features in the harmonic spectrum. The latter can only be explained if the coherent nature of the interaction is taken into account. Previous studies showed similar characteristics in the HHG of He^+ ions when the process starts from a coherent superposition of two states [36]. In [36], however, it was not stated how to prepare the system in such a coherent superposition and a simple two-level system as model was used.

The manuscript is organized as follows. In Section 2, we introduce the CPR technique and its main features. We illustrate the time dependent population transition between two bound states via a long laser pulse which has a frequency out of resonance. In Section 3, we present our one-dimensional model and the results of the HHG emission for different parameters. Section 4 is devoted to the extension of the predictions of Section 3 to a full 3D-TDSE model. This allows us both to confirm our outcomes and to have available a powerful theoretical tool to use in comparison with experiments. Finally, in Section 5, we complete our contribution with a brief summary and an outlook.

2 Coherent population return (CPR) technique

In the following we review the basic concepts of CPR paying special attention to the possibility of using this coherent technique for the preparation of an active medium. Let us consider a two-level quantum system of bare states ψ_1 and ψ_2, excited by a pump radiation pulse detuned from resonance by an amount $\Delta = E_{21} - \omega_L$, where $E_{21} = E_2 - E_1$ is the energy gap between both states and ω_L the carrier frequency of the pump laser pulse. The Hamiltonian that describes this situation after Rotating Wave Approximation (RWA) [37] can be written as

$$H(t) = \frac{1}{2}\begin{bmatrix} 0 & \Omega(t) \\ \Omega(t) & 2\Delta \end{bmatrix}, \tag{1}$$

where Ω is the Rabi frequency. In an adiabatic basis, i.e., in the basis that diagonalize the Hamiltonian of equation (1), the instantaneous eigenstates read

$$\begin{aligned} \Phi_+(t) &= \psi_1 \sin\vartheta(t) + \psi_2 \cos\vartheta(t) \\ \Phi_-(t) &= \psi_1 \cos\vartheta(t) - \psi_2 \sin\vartheta(t), \end{aligned} \tag{2}$$

with the mixing angle defined by $\vartheta(t) = (1/2)\arctan[\Omega(t)/\Delta]$. It can be shown that if $|\Delta| \gtrsim 1/\tau$, where τ is the pump pulse duration, the evolution of the system is adiabatic [33]. Thus, if the statevector of the system $\Psi(t)$ is initially aligned with one of the adiabatic eigenstates, i.e., $\Phi_+(t)$ or $\Phi_-(t)$, it will remain parallel during the whole excitation process. Let us suppose the adiabatic condition ($|\Delta| \gtrsim 1/\tau$) is fulfilled, and that at the beginning of the interaction all the population starts in the ground (lower) state. Hence we can write $\Psi(t) = \Phi_-(t) = \psi_1$ since

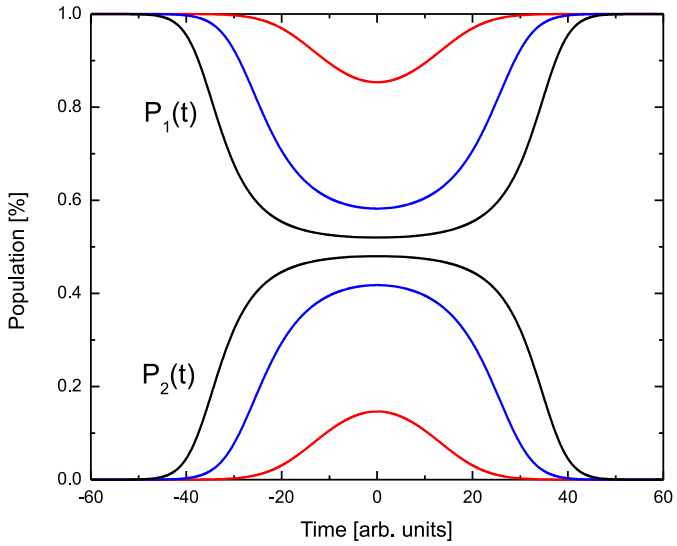

Fig. 1. Population of the excited and ground states versus time for different Ω_0/Δ ratios. The Rabi frequency is $\Omega(t) = \Omega_0 \exp(-t^2/\tau^2)$ with $\tau = 20$ a.u. The red case corresponds to a Ω_0/Δ ratio of 1, the blue case to $\Omega_0/\Delta = 6$, and the black case to $\Omega_0/\Delta = 25$.

$t = -\infty \rightarrow \Omega(-\infty) = 0 \rightarrow \vartheta(-\infty) = 0$. During the interaction, i.e., $-\infty < t < +\infty \rightarrow \Omega(t) \neq 0 \rightarrow \vartheta(t) \neq 0$, $\Psi(t)$ is a coherent superposition of the bare states ψ_1 and ψ_2, therefore some population is being excited to the upper state $\Phi_+(t)$. Once the interaction has ceased, i.e., $t = +\infty \rightarrow \Omega(+\infty) = 0 \rightarrow \vartheta(+\infty) = 0$, the statevector of the system reads again $\Psi(+\infty) = \Phi_-(+\infty) = \psi_1$. According to this last reasoning, the population transferred to the excited state during the process returns completely to the ground state once the interaction has finished. As a consequence, no population resides permanently in the excited state, no matter how large the transient intensity of the laser pump pulse might be.

Following the previous analysis we can write the population of the excited state during the interaction as

$$P_2(t) = \sin^2 \vartheta(t) = \frac{1}{2} - \frac{1}{2\sqrt{(\Omega(t)/\Delta)^2 + 1}}, \qquad (3)$$

where we can observe how it is possible to obtain $P_2 \rightarrow 1/2$ during the center part of the interaction for $\Omega(t) \gg \Delta$, reaching therefore a maximum coherent superposition of the quantum states. In order to illustrate these facts, Figure 1 shows the population of both the ground and excited states for different Rabi frequencies maintaining the detuning Δ fixed. It can be seen that for increasing the excitation intensity the population tends to be equally distributed between the ground and excited states, therefore achieving a perfect coherent superposition of these both states during the central part of the excitation laser pulse.

It is worth to mention that in a real situation the use of the CPR technique for obtaining a maximum superposition is limited by the possible ionization of the system when increasing the Rabi frequency, i.e., when the peak excitation intensity increases. According to this fact, it is much more convenient to use long pulses, e.g. nanosecond or picosecond, rather than short ones, e.g. few-femtoseconds. This is so because, although long pulses present a much smaller peak intensity than the short ones, they couple transitions between bound states much stronger. A simple way to understand this affirmation is to take into account that short pulses have associated broad frequency bandwidths, being these bandwidths usually much larger than the natural ones of atomic states. Thus, the part of the laser bandwidth on resonance with a certain transition, i.e. the effective bandwidth, is small when compared with long laser pulses, e.g. ns pulses, where the laser bandwidth and the natural bandwidth of the states are comparable.

3 One-dimensional model

Firstly, and for simplicity, the ideas discussed in the previous Section are implemented in a one-dimensional model using a short-range potential. We should to stress out, however, that our predictions could be extended to long-range potentials. Studies about the influence of the model potential in resonance-enhanced HHG were carried out by Figueira de Morisson Faria et al. [38] and it was shown similar behavior for both short and long-range potentials. This is related with the fact that the channel closings typical of a short-range potential are capable of generating essentially the same effects that the long-range ones. In addition, the energy structure in a short-range potential is more flexible and easy to manipulate and this allow us to choose the parameters in such a way to avoid spurious contributions. As a prototypical short-range potential we use the so-called Pöschl-Teller potential:

$$V(x) = -(1/2)\lambda(\lambda+1)\mathrm{sech}^2 \xi x, \qquad (4)$$

where ξ is the screening charge length and λ is a parameter related to the potential depth. We use here $\lambda = 7$ and $\xi = 0.15$. The bound eigenfunctions ψ_μ with eigenvalues E_μ are given by [39]

$$\psi_\mu = P_\lambda^\mu(\tanh \xi x),$$
$$E_\mu = -\xi^2 \mu^2/2 \ \text{ with } \ \mu = \lambda, \lambda-1, \ldots, 1, \qquad (5)$$

where $P_\lambda^\mu(\tanh \xi x)$ are the associated Legendre polynomials. It is important to mention that the parameters λ and ξ are chosen in a way that no Bohr frequency between bounds states coincide with the frequency of any harmonic of the fundamental laser. Otherwise, the harmonic generation at this precise frequencies would be enhanced disguising therefore the real enhancement produced by the coherent superposition of states. For such parameters λ and ξ, the ground and the first excited states energies are $E_1 = -0.55125$ a.u. and $E_2 = -0.405$ a.u., respectively.

The spectral intensity of the harmonic emission, $I_{\mathrm{HHG}}(\omega) = |a_x(\omega)|^2$, is defined via the Fourier transform

of the electron dipole acceleration $a_x(t)$:

$$I_{\mathrm{HHG}}(\omega) = \frac{1}{2\pi}\left|\int_{-\infty}^{+\infty} a_x(t)e^{i\omega t}dt\right|^2, \quad (6)$$

with $a_x(t) = \langle\psi(t)|E(t) + \frac{\partial}{\partial x}V(x)|\psi(t)\rangle$. To compute the expectation value $a_x(t)$ the space-time electronic wavefunction $\psi(x,t)$ needs to be calculated. To this end we obtain $\psi(x,t)$ by numerically integrating the TDSE in 1D:

$$H\psi(x,t) = i\frac{\partial}{\partial t}\psi(x,t), \quad (7)$$

where $H = H_0 + V_{\mathrm{int}}(x,t)$ is the full Hamiltonian operator of the system. It includes the field-free Hamiltonian, H_0, and the laser-electron coupling $V_{\mathrm{int}}(x,t) = x\,[E_{\mathrm{CPR}}(t) + E_{\mathrm{IR}}(t)]$ that defines the interaction of the CPR, $E_{\mathrm{CPR}}(t)$, and IR, $E_{\mathrm{IR}}(t)$, laser pulses with the electron under the dipole approximation (note the length gauge is used throughout our numerical model).

We have implemented the split-operator method [40] to numerically integrate equation (7) such as in the QFISHBOWL library [41]. This implementation is written in C++ programming language and uses the fast Fourier transform (FFT) [42] to solve the TDSE under a pseudo-spectral scheme.

Figure 2 shows the harmonic spectrum computed via equation (6) for the situation where the CPR laser pulse, prepares the system in a coherent superposition between the ground and first excited states of the above described Pöschl-Teller potential (see Eq. (4)). Second, an infrared (IR), laser pulse produces the harmonic emission. The laser electric fields used in the simulation are:

$$E_{\mathrm{CPR}}(t) = \epsilon_0 \exp\left(-(t-t_0)^2/\tau^2\right)\sin\left(\omega_0(t-t_0) - \phi_0\right), \quad (8)$$

with $\epsilon_0 = 1\times10^{-4}$ a.u., $\omega_0 = 0.14620$ a.u., that correspond to a wavelength of $\lambda_{\mathrm{CPR}} = 320$ nm and a detuning of $\Delta = 5\times10^{-5}$ a.u., $\tau = 1\times10^5$ a.u. (2.42 ps FWHM), $t_0 = 2.196\times10^5$ a.u. and carrier envelope phase $\phi_0 = 0$ rad and

$$E_{\mathrm{IR}}(t) = \epsilon_1 \cos^2\left[\frac{\omega_1}{2N}(t-t_1)\right]\cos\left[\omega_1(t-t_1) - \phi_1\right], \quad (9)$$

where the electric field $E_{\mathrm{IR}}(t)$ becomes zero when $t < t_1 - \frac{\pi N}{\omega_1}$ and $t > t_1 + \frac{\pi N}{\omega_1}$ and t_1 denotes the time for the maximum peak amplitude of the IR electric field envelope. Then, we define the delay, τ_d, between the CPR and IR pulses as $\tau_d = t_1 - t_0$. The peak amplitude of the IR laser electric field is $\epsilon_1 = 0.03$ a.u. (corresponding to an intensity of $\approx 3.16\times10^{13}$ W/cm^2), the central frequency, $\omega_1 = 0.057$ a.u. (corresponding to a wavelength $\lambda_{\mathrm{IR}} = 800$ nm), and the number of cycles, $N = 10$ (i.e. a total time duration of around 30 fs). For the present simulation, we set the delay τ_d and the carrier envelope phase ϕ_1 equal to zero. We have made simulations for other values of τ_d (not shown in the present article) in order to show how sensitive is the harmonic emission yield to this parameter. Slightly changes are observed and only with larger values of τ_d, of the order of the FWHM of the CPR laser, appreciable variations are noticed. The analysis of these modifications, however, is out of the scope of the present work.

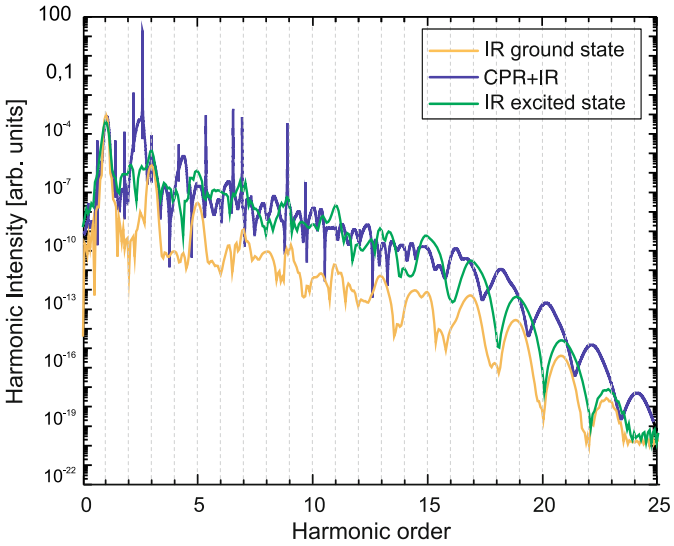

Fig. 2. Harmonic emission from a coherent superposition of states induced by CPR (blue line), from the ground state (orange line), and from the excited state (green line). For the latter two cases only the IR laser pulse is used. The parameters for the simulations are: CPR laser $\epsilon_0 = 1\times10^{-4}$ a.u., $\omega_0 = 0.14620$ a.u. (corresponding to a detuning of $\Delta = 5\times10^{-5}$ a.u.), and $\tau = 1\times10^5$ a.u., IR laser $\epsilon_1 = 0.03$ a.u., $\omega_1 = 0.057$ a.u., and $N = 10$ (see the text for more details). The integration time window is 5τ with time step $\Delta t = 0.25$ a.u., and the position grid length $L_x = 1\times10^5$ a.u. with $\Delta x = 0.5$ a.u.

Furthermore, Figure 2 clearly shows that an enhancement in the harmonic emission is obtained when the medium is previously prepared in a coherent superposition of states compared to the case where only one state is used. The HHG spectrum from the first excited state driven by only the IR laser is shown in the same figure as well. As the ionization yield is larger from the excited state with respect to the ground state, it can be expected that the recombination process is more efficient. Therefore, the HHG spectra is enhanced when the system is driven by the IR alone from the first excited state. Along the text, we will explain in more detail the role of the CPR laser in the preparation of the coherent superposition of the ground and first excited states and what is the behaviour of the HHG spectra for such a case.

For a better understanding of this fact, Figure 3 shows the population dynamics of the ground and first excited states when both lasers interact with the system. In the first part of the interaction, the CPR laser creates adiabatically the coherent superposition of states. When this superposition is maximum, the IR laser drives the harmonic emission with the consequent enhancement of the harmonic yield. It is important to point out that the intensity of the CPR laser is not enough for inducing any multiphoton process that could enhance the harmonic emission for itself. According to equation (3) the population of the

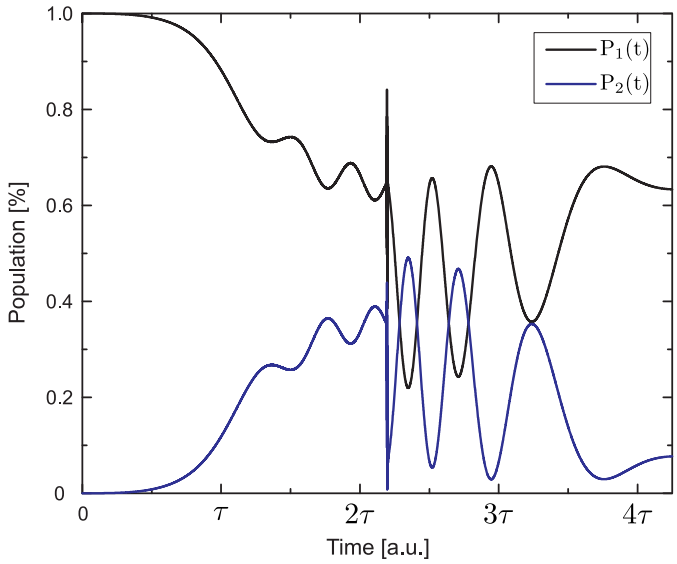

Fig. 3. Population dynamics of the ground (black line) and first excited states (blue line). The pulses parameter are the same as in the simulation depicted in Figure 2.

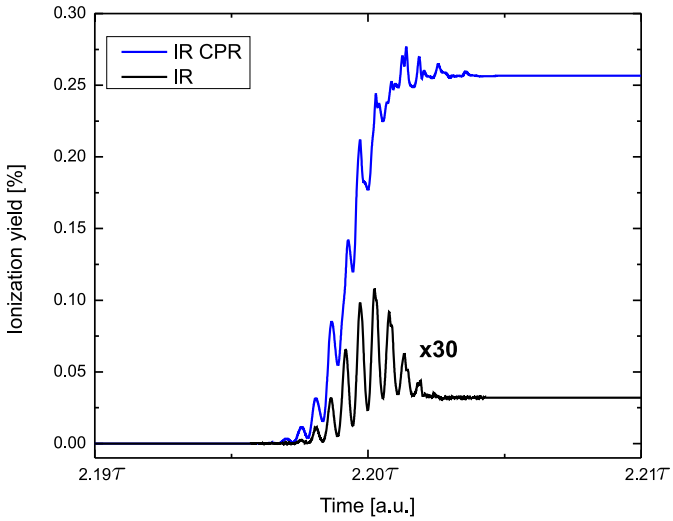

Fig. 4. Ionization yield when only the IR laser interacts with the system (black case), and the combination CPR+IR (blue case). The ionization is calculated by projecting out the first three bound states from the whole wavefunction of the system $\Psi(x,t)$.

excited state during the CPR process depends only on the ratio $\Omega(t)/\Delta$, being Δ limited by the adiabatic condition $|\Delta| \gtrsim 1/\tau$. Therefore for long temporal pulses the detuning of the CPR laser from the Bohr frequency of the selected transition is reduced, and accordingly the required Rabi frequency.

The origin of the harmonic enhancement can be understood following the analysis carried out by Watson et al. in [21]. Let us assume that once the coherent superposition with coefficients $\alpha(t)$ and $\beta(t)$ is generated by the CPR laser, i.e.,

$$|\Psi(t)\rangle = \alpha(t)|\Psi_1(t)\rangle + \beta(t)|\Psi_2(t)\rangle, \tag{10}$$

the IR laser can partially ionize both states. Then, according to the Lewenstein model [11], the states $|\Psi_1(t)\rangle$ and $|\Psi_2(t)\rangle$ can be written as:

$$\begin{aligned}|\Psi_1(t)\rangle &= a_1(t)|\psi_1\rangle e^{-iE_1 t} + \int dn b_n(t) e^{-i\omega_n t}|\psi_n\rangle,\\ |\Psi_2(t)\rangle &= a_2(t)|\psi_2\rangle e^{-iE_2 t} + \int dn' b'_{n'}(t) e^{-i\omega_{n'} t}|\psi_{n'}\rangle,\end{aligned} \tag{11}$$

where the variables $a_1(t)$ and $a_2(t)$ describe the evolution of the population of the two bound states, and the coefficients $b_n(t)$ and $b'_{n'}(t)$, denote the complex amplitudes of the continuum states $|\psi_n\rangle$ and $|\psi'_n\rangle$, respectively.

According to the results of the ionization yield depicted in Figure 4, we assume that the ionization amplitude from the ground state is too small compared to the ionization of the excited state, $|b_n(t)|^2 \ll |b'_{n'}(t)|^2$. Thus, the vector state of the system, $|\Psi(t)\rangle$, reads

$$\begin{aligned}|\Psi(t)\rangle \approx \alpha(t)|\psi_1\rangle e^{-iE_1 t}\\ + \beta(t)\left[a_2(t)|\psi_2\rangle e^{-iE_2 t} + \int dn' b'_{n'}(t) e^{-i\omega_{n'} t}|\psi_{n'}\rangle\right],\end{aligned} \tag{12}$$

where we have set $a_1(t) = 1$. This is so because $\alpha(t)$ describes the population of the ground state $|\psi_1\rangle$.

As it was stated at the introduction of this section, the harmonic spectrum is proportional to the Fourier transform of the dipole acceleration $a_x(t) = \langle\Psi(t)|\hat{a}_x|\Psi(t)\rangle$, and, according to equation (12) we can write

$$\begin{aligned}a_x(t) = |\beta(t)|^2 \int dn' a_2^*(t) b'_{n'}(t)\langle\psi_2|\hat{a}_x|\psi_{n'}\rangle e^{-i(\omega_{n'} - E_2)t}\\ + \alpha^*(t)\beta(t) a_2(t)\langle\psi_1|\hat{a}_x|\psi_2\rangle e^{-i(E_2 - E_1)t}\\ + \alpha^*(t)\beta(t)\int dn' b'_{n'}(t)\langle\psi_1|\hat{a}_x|\psi_{n'}\rangle e^{-i(\omega_{n'} - E_1)t} + \text{c.c},\end{aligned} \tag{13}$$

where the dipolar acceleration operator is denoted by $\hat{a}_x = \frac{\partial}{\partial x}V(x) + E_{\text{IR}}(t)$. For simplicity in the derivation of equation (13), we have neglected the terms due to the continuum-continuum transitions. The first and third terms in equation (13) describe the dipole acceleration when the electron recombines with the excited state and the ground state, respectively, while the second term is related with transitions between the bound states.

Several interesting facts can also be extracted analyzing in detail the equation (13). First of all, we need to take into account that ionization mechanisms are much more efficient from the excited state than from the ground one.

As a consequence, when the system is prepared in a superposition of states it is expected a much larger ionization (see Fig. 4). It is important to point out that the enhancement of the ionization yield shown in Figure 4 is produced not only by an enhancement in the multiphoton ionization probability. The multiphoton ionization from the ground state requires the absorption of at least ten IR photons whilst from the excited state eight photons are required, but also this is so for the tunneling ionization probability. The relation between the Keldysh parameters from ground and excited states is $\gamma_{\text{Exc.}}/\gamma_{\text{Ground}} \simeq 0.86$. Thus, and according to the integral terms of equation (13), it is clear that the total dipole acceleration is enhanced when compared to the acceleration contribution of a situation where the medium is not previously prepared.

Another feature that deserves attention is the shift in energy, more clearly seen for high-order harmonics, of the emission in the CPR+IR case when compared to the IR alone (see Fig. 2). This energy shift was predicted by Burnett et al. in reference [21] for the harmonic emission of a coherent superposition of states and quantified as the energy difference between these states. This shift can be easily understood assuming that the different coefficients of equation (13) are slowly varying functions of time. Hence, the integral terms in equation (13), which are those related by the recombination of the electron, differ by a factor

$$e^{-i(E_2-E_1)t}, \tag{14}$$

which corresponds to the energy gap between the ground and excited states. Thus, for the harmonics generated from a coherent superposition of states, a double harmonic structure shifted by the energy difference between the states of the superposition and modulated by the ionization probability must be observed.

Furthermore, as it can be clearly seen in Figure 2, besides of the typical structure of harmonics generated by the IR laser, there is superimposed a much sharper structure at the low-order harmonics region. According to the second term of equation (13),

$$\alpha^* \beta a_2 \langle \psi_1 | \hat{a}_x | \psi_2 \rangle e^{-i(E_2-E_1)t}, \tag{15}$$

it is expected that at the Bohr frequency of the transition between the states coupled by the CPR pulse, i.e., the two first states, to find an enhancement in the harmonic emission. This transition corresponds to an energy of $E_2 - E_1 = 0.14625$ a.u. and harmonic order of ~ 2.57. The corresponding emission is clearly seen in Figure 2 and in fact it is the most intense one. Moreover, if the analysis of CPR carried out previously is extended beyond a two-level system, the harmonic spectrum will contain terms corresponding to the energy difference of all pair of states that are optically accessible. Although the contribution of these other pair of states is rather small when compared with the combination between ground and excited states (the detuning is much larger, see Eq. (3)), there is still a clear signature of such coherent preparation in the harmonic emission.

For a better understanding of the above cited fact, in Table 1 we present the harmonic order of all possible

Table 1. Harmonic order for all the possible pairs of states optically accessible.

$\lvert E_i - E_j \rvert/\omega_1$	ψ_1	ψ_2	ψ_3	ψ_4	ψ_5	ψ_6	ψ_7
ψ_1	x	2.57	x	6.51	x	8.88	x
ψ_2	2.57	x	2.17	x	5.33	x	6.91
ψ_3	x	2.17	x	1.78	x	4.14	x
ψ_4	6.51	x	1.78	x	1.38	x	2.96
ψ_5	x	5.33	x	1.38	x	1.01	x
ψ_6	8.88	x	4.14	x	1.01	x	0.59
ψ_7	x	6.91	x	2.96	x	0.59	x

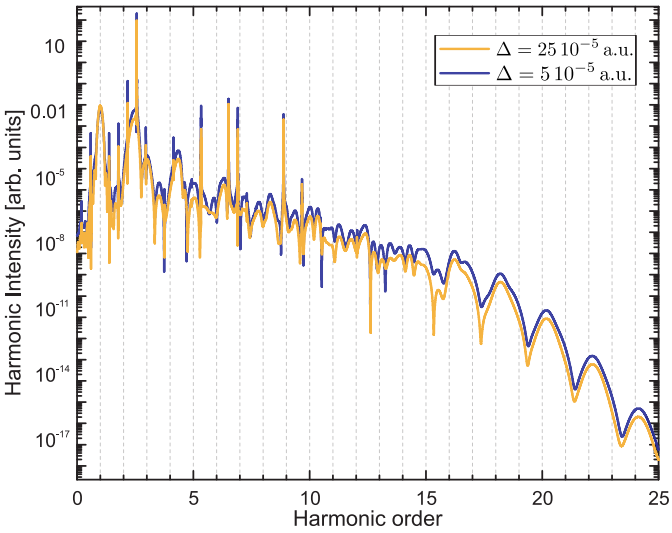

Fig. 5. Harmonic emission as a function of the detuning of the CPR laser. The laser parameters were those of Figure 2 except the central frequency of the CPR laser pulse that was set now to $\omega_0 = 0.14600$ a.u.

combinations. Comparing the sharp structure for low harmonics shown in Figure 2 with the values of Table 1, it is possible to conclude that the enhancement for low-order harmonics it is mainly produced by the interference term of equation (15) rather than by the higher ionization probability discussed previously. It is important to stress out that the latter effect is a purely coherent (quantum) effect with no analogy in classical Physics.

In order to check that the enhancement in the harmonic emission is directly related to the coherent superposition created by the CPR laser, Figure 5 shows the harmonic emission for different detunings of the CPR laser, i.e., for different carrier frequencies, with the same parameters as in Figure 2. According to equation (3) if Δ increases, the population transferred to the excited state P_2 decreases, and accordingly the coherence induced in the system. This can be clearly seen in Figure 5 where for larger detunings Δ the harmonic emission produced by the IR laser decreases.

It is also important to verify that this effect is independent of the intensity of the IR laser employed for the harmonic generation. For every different intensity used in

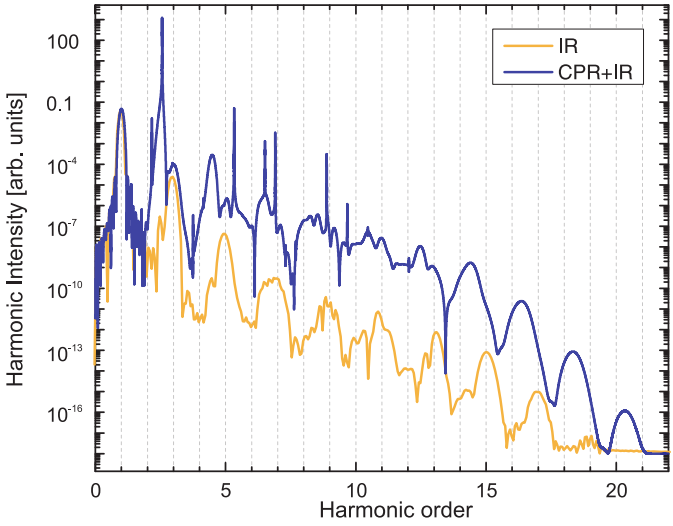

Fig. 6. High harmonic emission from a coherent superposition of states produced by CPR (blue line), compared with no superposition (orange line), i.e. where only the IR laser is present. The IR laser peak electric field is $\epsilon_1 = 0.02$ a.u. The other parameters are the same as in Figure 2.

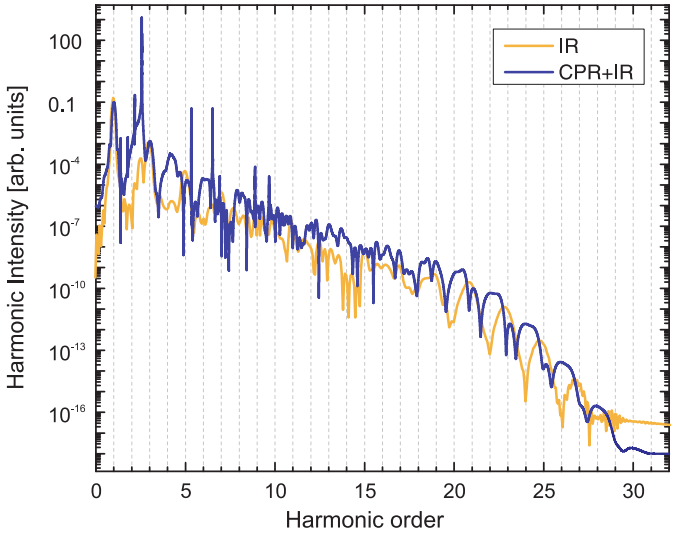

Fig. 7. Harmonic emission from a coherent superposition of states produced by CPR (blue line), compared with the case where it is not superposition (orange line), i.e. where only the IR laser is present. The IR laser peak electric field is $\epsilon_1 = 0.04$ a.u. The other parameters are the same as in Figure 2.

this work, there is a clear enhancement in the harmonic emission once the active medium has been previously prepared in a coherent superposition of states. To illustrate this fact Figures 6 and 7 show the harmonic emission when the IR laser electric field is set to 0.02 and 0.04 a.u., respectively. For both cases the CPR laser has the parameters indicated for Figure 2. Although for Figure 7 the emission is reduced, there is still an improvement with respect to the situation where no CPR laser is present. According to Platonenko and coworkers [43,44] the harmonic yield emission decreases when the IR laser electromagnetic field intensity increases. The electron wave packet *spreading* increases and the recombination cross section then decreases as a function of the IR laser field intensity. This fact explains the reduction in the enhancement of the harmonic emission between the CPR+IR and the IR cases shown in Figure 7. Note that the HHG emission for the cases depicted in Figures 2, 6 and 7, show the same cutoff harmonic shift between the two spectra. This clearly indicates that such shift is independent of the IR laser field intensity and has its origin in the coherent superposition of states. The situation studied in reference [21] differs, however, from the one presented in this manuscript because, as it was stated before, the CPR laser induces a coherent superposition of all the states of the system. Nevertheless, the energy shift can be distinctly related with the coherence induced in the system.

In order to obtain deeper insight about the laser electron dynamics, Figure 8 shows the electronic density as a function of position and time around the maximum electromagnetic field of the IR and CPR+IR laser pulses, respectively. It is interesting to notice that qualitatively there is not a significant difference in the re-collision events when the IR or the combination CPR+IR lasers act over the system. However, the main part of the electronic density presents a completely different behavior for both situations being much more complex for the lower frame of Figure 8 than for the upper one. It is worth to mention that when both frames are compared, the ionization events, as well as the re-collision wavepacket, show larger enhancements for the case of CPR+IR compared to the IR alone. This can be explained taking into account that when the medium is prepared in a coherent superposition, the IR laser field will mainly ionize the electron from the first excited state rather than from the ground state. This is well understood by considering that the second state is in barrier suppression regime, while the ground state is still close to the tunnelling regime, for the intensity used in the simulation of Figure 8.

In a next step we have used time-analysis tools to characterize the HHG spectra calculated using our quantum one-dimensional model. To this end, we have employed the Gabor transformation, developed in the 40's by Gabor [45], which has proven to be a very efficient numerical tool to estimate the emission times of HHG in atoms and molecules and to discriminate between the different electron trajectories [46].

Figure 9 shows the time-frequency spectrogram when the IR pulse (upper frame) and the combination of CPR and IR pulses (lower frame) produce the HHG emission. In the case where the IR laser alone drives the system, we note that the cutoff is not strictly abrupt (see Fig. 2), but it is defined from the 15th to the 21st harmonic approximately. This harmonic region shows only one recollision event, i.e., only one short and long trajectories contributes to the harmonic emission. An absence of interferences, i.e. an almost clear continuum, is visible for this region in the spectrum of Figure 2. It is important to point out that exists a nonzero probability to find interferences in the

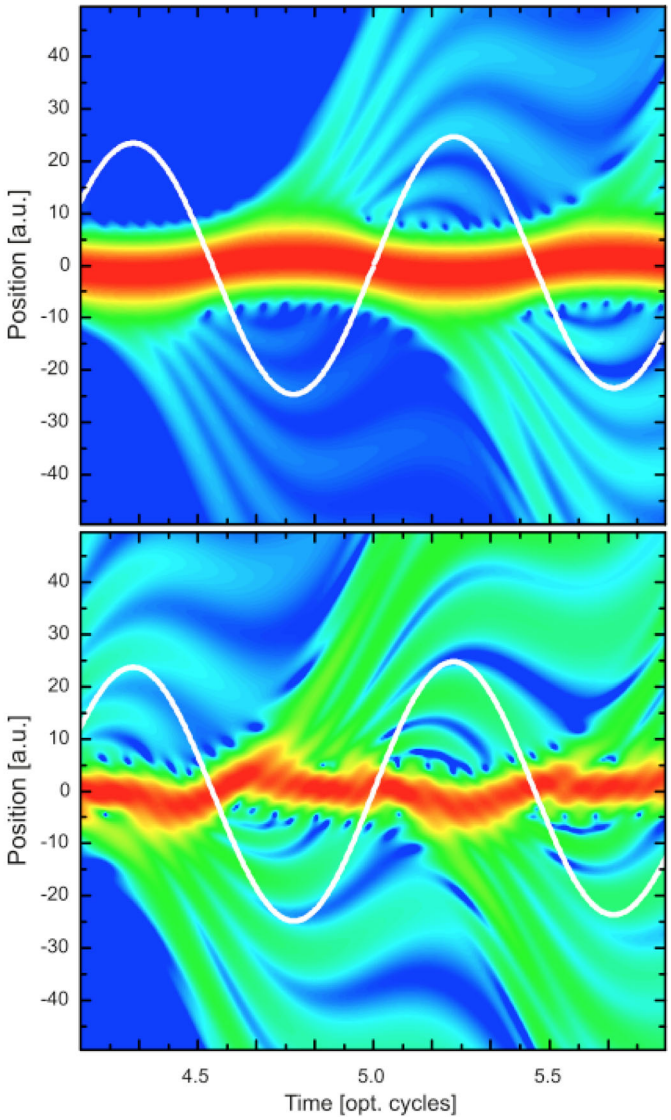

Fig. 8. Upper frame: electronic density as a function of position and time when only the IR laser electric field (white line) interacts with the system. Lower frame: both CPR and IR lasers interact with the system. The data for the simulation are the same as those of Figure 2.

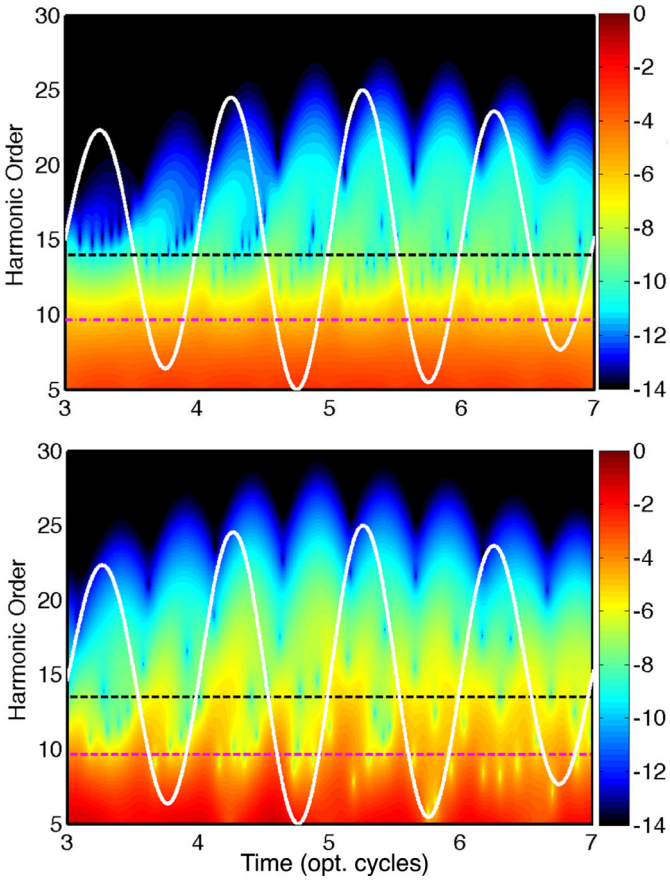

Fig. 9. Logarithm of the spectrogram of Gabor's distributions (in color scale) of the HHG emission for the case of IR (upper frame) and CPR+IR (lower frame). The white solid line corresponds to the IR laser field. The horizontal lines denote the cutoff (black dashed) harmonic energy and the ionization potential of the ground state (magenta dashed with point), respectively. The data for the simulation are those of Figure 2.

energy region between the ionization potential and cutoff energy of the harmonic spectra. This feature appears due to the fact that several trajectories contribute to the HHG emission [11]. In clear contrast to the above mentioned facts, the region between the 5th to the 15th harmonic presents a much richer structure and this is related to the interference between the contribution coming from different electron trajectories.

Furthermore, as predicted by previous simulations, the enhancement in the harmonic emission is clearly shown when the medium is coherently prepared prior to the HHG emission. Although the spectrograms are similar for the harmonic emission events in both cases, there are significant differences in the time window between 5–7 opt. cycles (compare the upper and lower frames in Fig. 9). It is important to notice that in both spectrograms it is hard to distinguish between the long and short trajectories contribution to the HHG. In addition, even when an interference structure is hardly visible in Fig. 9), we can clearly see noticeable differences between the two panels. They come from the different recollision events of the short and long trajectories due to both recombination channels, i.e., the ground and first excited states (integral terms in Eq. (13)). Moreover, the distinct structure below the ionization potential of the ground state is explained by the fact that the electron can recombine with the excited state too. Then, short and long trajectories seem to interfere in the region between approximately 5th and 9th harmonics.

4 Three-dimensional model

In order to check that the results previously discussed are not an artifact caused by the dimensionality of the problem, we have also developed a three-dimensional model

utilizing the same Pöschl-Teller potential:

$$V(r) = -\frac{1}{2}\lambda(\lambda+1)\xi^2 \mathrm{sech}^2(\xi r), \quad (16)$$

with $\lambda = 7.565$ a.u. and $\xi = 0.160$ a.u. It is worth noticing that we have tuned slightly the potential parameters in order to obtain a similar energy spectra for both the 1D and 3D cases.

We have used the spectral split-operator method in spherical coordinates presented in [47], to solve the 3D-TDSE. By considering the problem has spherical symmetry and the laser electric field is linearly polarized, in particular along the z-axis, the quantum magnetic momentum m is equal to zero and the effective potential does not depend on the azimuthal angle ϕ. This fact allows us to solve the TDSE under the radial r and polar coordinates θ without losing any 3D effect in our calculation.

The code employed to solve the TDSE in spherical coordinates is called Quantum-Sphere-TDSE and it was written in C++ (see [48] for more details). Here, the pseudo-spectral algorithm employs the Fast Fourier Transform (FFT) to solve the TDSE along the radial coordinate r and the Fast Legendre Transform [49], along the polar coordinate θ (see e.g. [47]).

The bound states were computed by imaginary time propagation [50]. The resulting energies for the first two bound states, i.e., the orbitals $1s$ and $2p$, are -0.552 a.u. and -0.389 a.u., respectively. The imaginary time step is set to $\Delta t = -0.05i$ a.u. and for the space grids we use $\Delta r = 0.3$ a.u., with $N_r = 540$ along the radial coordinate r, and an angular step $\Delta\theta = 0.024544$ rad, with $N_\theta = 128$ along the θ coordinate.

To simulate the HHG emission by the 3D numerical solution of the TDSE under similar condition of the 1D results, we have reduced the time duration of the CPR and IR laser pulses. Consequently, for the 3D case the CPR pulse is substantially shorter than for the 1D one. This is so to optimize the computational time of the simulation. Otherwise the temporal window becomes too broad and extremely difficult to handle numerically. This change must have almost no influence in the simulation results because, as it was stated above, CPR is insensitive to the pulse duration provided that the adiabatic condition is fulfilled.

For the present simulations, the CPR laser pulse is described by equation (8) with $\epsilon_0 = 26 \times 10^{-4}$ a.u., $\omega_0 = 0.161$ a.u., (corresponding to a detuning of $\Delta = 2 \times 10^{-3}$ a.u.) and $\tau = 8.8 \times 10^3$ a.u. (0.213 ps). The IR laser pulse is defined as in equation (9) with $\epsilon_1 = 0.03$ a.u., $\omega_1 = 0.057$ a.u. and $N = 4$. The space grid used is the same that in the bound state calculation, we changed, however, the number of points to $N_r = 15\,400$ along the radial coordinate r and the time step is set to $\Delta t = 0.05$ a.u. Finally, to avoid the unphysical reflections of the wavefunction at the grid border, we employ a boundary mask function $\cos^{1/6}$ in the final 5% of the position grid size along the radial coordinate r.

Figure 10 shows the harmonic emission spectra for the IR and the CPR+IR cases obtained by numerical integration of the 3D-TDSE. As it can be seen the results are

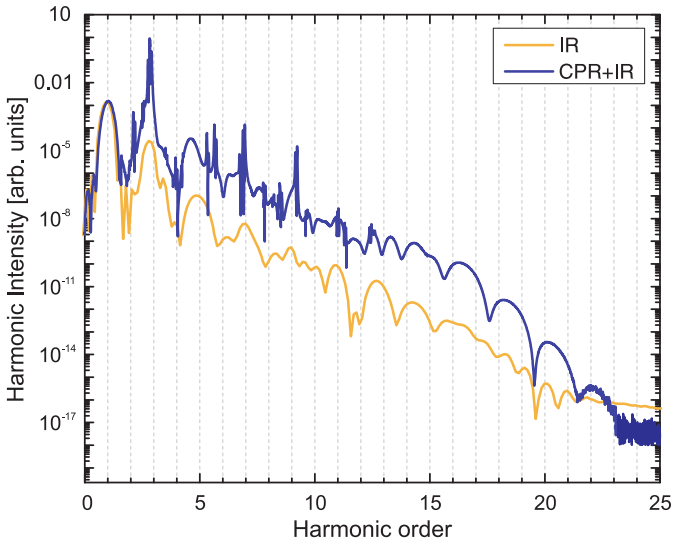

Fig. 10. 3D-TDSE calculation for the high harmonic emission from a coherent superposition of states produced by CPR (blue line), compared with no superposition (orange line), i.e. where only the IR laser is present. The data for the simulation are: CPR laser $\epsilon_0 = 26 \times 10^{-4}$ a.u., $\omega_0 = 0.161$ a.u. (corresponding to a detuning of $\Delta = 2 \times 10^{-3}$ a.u.), and $\tau = 8.8 \times 10^3$ a.u., IR laser $\epsilon_1 = 0.03$ a.u., $\omega_1 = 0.057$ a.u., and $N = 4$.

in clear qualitative agreement with the 1D-TDSE, discarding therefore any effect of the dimensionality of the simulations in the enhancement of the harmonic emission discussed before. The minor differences between the 1D and 3D simulations are mainly caused by the widening of the electronic density for the 3D case perpendicular to the polarization direction. Thus, the recombination becomes less efficient and the harmonic yield can be different when compared to the 1D situation. Contrarily to the 1D result, the cutoff region of the Figure 10 is close to be continuum. This fact can be easily understood taking into account that the IR electromagnetic field is shorter than in the 1D case. Considering different laser parameters are used in the 3D calculations, the cutoff structure of the HHG spectra differs from the presented in the 1D case. To obtain the same 1D structural behaviour in our 3D model, a large integration spatial grid will be required. Therefore, extensive numerical calculations will be needed and this would make the computation of HHG spectra difficult in a reasonable computational time.

5 Conclusions and outlook

In this manuscript we have presented a simple and robust scheme for the efficient generation of high-order harmonics. This scheme is based on the preparation of the active medium in a coherent superposition of states before driving it with an intense IR laser pulse. Our numerical results, based both in reduced and full dimensionality approaches, show that the emission of the HHG is clearly enhanced when the medium is coherently prepared utilizing the CPR technique.

For high-order harmonic this enhancement can be understood by attending to the higher ionization probability of the excited state, when compared with the ground state. On the other hand, for low-order harmonics, the interference term resulting from generating harmonics starting from a coherent superposition of states is the responsible of the emission enhancement. It is important to notice that this interference term not only produce an enhancement at the Bohr frequency between the ground and first excited states, but in addition at the frequencies of all the possible optical transitions in the system. This rich structure in the harmonic emission has no classical analogy and is clearly produced by the coherence induced by the CPR laser.

For the experimental demonstration of the theoretical predictions of this manuscript Xe is a possible candidate. Similarly to the scheme used in Halfmann et al. in [35], laser radiation at a wavelength of 225 nm can be used to induce a two photon transition between the ground state $5p^6\ ^1S_0$ and the excited state $5p^57p^2\ [1/2]_0$ that have a lifetime of 30 ns. Once the 225 nm laser produces the superposition of states, the IR laser can be shined to produce the harmonic emission. Nevertheless we will like to emphasize that the analysis carried out in this paper is totally system independent. Thus, as long as the conditions for CPR are fulfilled and the superposition of states created, any media will offer an enhancement in the harmonic emission.

Finally we hope that this work will help not only to enhance the yield of the harmonic emission but also to explore new and distinct features based on coherent effects.

We are sincerely grateful to J.A. Pérez-Hernández, L. Plaja and L. Roso for the insightful discussion and useful suggestions. We thank to R Morán for useful discussion in the C++ programming implementation of the 3D-TDSE. A.C. thanks the Secretaría Nacional de Ciencia Innovación y Innovación (SENACYT) Panamá and the Spanish Ministry Project FrOntiers of QUantum Sciences (FOQUS): Atoms, Molecules, Photons and Quantum Information (FIS2013-46768-P) for financial support. We also acknowledge the support from the EC's Seventh Framework Programme LASERLAB-EUROPE III (grant agreement 284464) and the Ministerio de Economía y Competitividad of Spain (FURIAM project FIS2013-47741-R).

References

1. M. Drescher, M. Hentschel, R. Kienberger, M. Uiberacker, Y. Yakovlev, A. Scrinzi, Th. Westerwalbesloh, U. Kleineberg, U. Heinzmann, F. Krausz, Nature **419**, 803 (2001)
2. M. Uiberacker, M.T. Uphues, M. Schultze, A.J. Verhoef, V. Yakovlev, M.F. Kling, J. Rauschenberger, N.M. Kabachnik, H. Schroder, M. Lezius, K.L. Kompa, H.G. Muller, M.J.J. Vrakking, S. Hendel, U. Kleineberg, U. Heinzmann, M. Drescher, F. Krausz, Nature **446**, 627 (2007)
3. A.L. Cavalieri, N. Müller, T. Uphues, V.S. Yakovlev, A. Baltuška, B. Horvath, B. Schmidt, L. Blümel, R. Holzwarth, S. Hendel, M. Drescher, U. Kleineberg, P.M. Echenique, R. Kienberger, F. Krausz, U. Heinzmann, Nature **449**, 1029 (2007)
4. A.N. Pfeiffer, C. Cirelli, M. Smolarski, R. Dörner, U. Keller, Nat. Phys. **7**, 428 (2011)
5. C. La-O-Vorakiat, M. Siemens, M.M. Murnane, H.C. Kapteyn, S. Mathias, M. Aeschlimann, P. Grychtol, R. Ada, C.M. Schneider, J.M. Shaw, H. Nembach, T.J. Silva, Phys. Rev. Lett. **103**, 257402 (2009)
6. A. Peralta Conde, J. Kruse, O. Faucher, P. Tzallas, E.P. Benis, D. Charalambidis, Phys. Rev. A **79**, 061405R (2009)
7. K. Kosma, S.A. Trushin, W. Fuss, W.E. Schmid, J. Phys. Chem. A **112**, 33 (2008)
8. T.K. Allison, T.W. Wright, A.M. Stooke, C. Khurmi, J. van Tilborg, Y. Liu, R.W. Falcone, A. Belkacem, Opt. Lett. **35**, 21 (2010)
9. P.B. Corkum, Phys. Rev. Lett. **71**, 1994 (1993)
10. P. Dietrich, N.H. Burnett, M. Ivanov, P.B. Corkum, Phys. Rev. A **50**, R3585 (1994)
11. M. Lewenstein, Ph. Balcou, M. Yu. Ivanov, A. L'Huillier, P.B. Corkum, Phys. Rev. A **49**, 2117 (1994)
12. J.A. Pérez-Hernández, M.F. Ciappina, M. Lewenstein, L. Roso, A. Zaïr A, Phys. Rev. Lett. **110**, 053001 (2013)
13. S. Haessler, T. Balčiunas, G. Fan, G. Andriukaitis, A. Pugžlys, A. Baltuška, T. Witting, R. Squibb, A. Zaïr, J.W.G. Tisch, J.P. Marangos, L.E. Chipperfield, Phys. Rev. X **4**, 021028 (2014)
14. C. Jin, G. Wang, H. Wei, A. Le, C.D. Lin, Nat. Commun. **5**, 4003 (2014)
15. J.A. Pérez-Hernández, L. Roso, A. Zaïr, L. Plaja, Opt. Exp. **19**, 19430 (2011)
16. J.A. Pérez-Hernández, D.J. Hoffmann, A. Zaïr, L.E. Chipperfield, L. Plaja, C. Ruiz, J.P. Marangos, L. Roso, J. Phys. B **42**, 134004 (2009)
17. J. Biegert, A. Heinrich, C.P. Hauri, W. Kornelis, P. Schlup, M.P. Anscombe, M.B. Gaarde, K.J. Schafer, U. Keller, J. Mod. Opt. **53**, 87 (2006)
18. B. Wang, T. Cheng, X. Li, P. Fu, S. Chen, J. Liu, Phys. Rev. A **72**, 063412 (2005)
19. C. Zhang, X. Liu, P. Ding, Y Qi, J. Math. Chem. **39**, 133 (2006)
20. L. Feng, T. Chu, Phys. Lett. A **376**, 1523 (2012)
21. J.B. Watson, A. Sanpera, X. Chen, K. Burnett, Phys. Rev. A **53**, 4 (1996)
22. F.I. Gauthey, C.H. Keitel, P.L. Knight, A. Maquet, Phys. Rev. A **52**, 1 (1995)
23. H. Niikura, D.M. Villeneuve, P.B. Corkum, Phys. Rev. Lett. **94**, 083003 (2005)
24. S. Chelkowski, T. Bredtmann, A.D. Bandrauk, Phys. Rev. A **88**, 033423 (2013)
25. M. Mohebbi, S. Batebi, J. Electron Spectrosc. **185**, 578 (2012)
26. P.M. Paul, T.I. Clatterbuck, C. Lynga, P. Colosimo, L.F. DiMauro, P. Agostini, K.C. Kulander, Phys. Rev. Lett. **94**, 113906 (2005)
27. P.M. Kraus, S.B. Zhang, A. Gijsbertsen, R.R. Lucchese, N. Rohringer, H.J. Wörner, Phys. Rev. Lett. **111**, 243005 (2013)
28. K. Bergamnn, H. Theuer, B.W. Shore, Rev. Mod. Phys. **70**, 1003 (1998)
29. A. Harris, Phys. Today **50**, 36 (1997)
30. J.P. Marangos, J. Mod. Opt. **45**, 3 (1998)
31. L.P. Yatsenko, B.W. Shore, N.V. Vitanov, K. Bergmann, Phys. Rev. A **68**, 043405 (2003)
32. A. Peralta Conde, L.P. Yatsenko, J. Klein, M. Oberst, T. Halfmann, Phys. Rev. A **72**, 053808 (2005)

33. N.V. Vitanov, B.W. Shore, L. Yatsenko, K. Böhmer, T. Halfmann, T. Rickes, K. Bergmann, Opt. Com. **199**, 117126 (2001)
34. A. Peralta Conde, L. Brandt, T. Halfmann, Phys. Rev. Lett. **97**, 243004 (2006)
35. S. Chakrabarti, H. Muench, T. Halfmann, Phys. Rev. A **82**, 063817 (2010)
36. J.B. Watson, A. Sanpera, X. Chen, K. Burnett, Phys. Rev. A **53**, R1962 (1996)
37. B.W. Shore, *The Theory of Coherent Atomic Excitation* (Wiley, New York, 1990)
38. C. Figueira de Morisson Faria, R. Kopold, W. Becker, J.M. Rost, Phys. Rev. A **65**, 023404 (2002)
39. G. Pöschl, E. Teller, Z. Phys. **83**, 143 (1933)
40. M.D. Feit, J.A. Fleck, A. Steiger, J. Comput. Phys. **47**, 412 (1982)
41. C. Ruiz, A. Chacón, QFISHBOWL library, http://code.google.com/p/qfishbowl
42. M. Frigo, S.G. Johnson, FFTW library, http://www.fftw.org
43. V.T. Platonenko, A.F. Sterjantov, V.V. Strelkov, Laser Phys. **14**, 443 (2003)
44. W.V. Fedorov, J. Peatross, Phys. Rev. A **52**, 504 (1995)
45. D. Gabor, J. Inst. Electr. Eng. **93**, 429 (1946)
46. C.C. Chirilă, I. Dreissigacker, E.V. van der Zwan, M. Lein, Phys. Rev. A **81**, 033412 (2010)
47. M.R. Hermann, J.A. Fleck, Phys. Rev. A **38**, 6000 (1998)
48. A. Chacón, R. Morán, QUANTUM-SPHERE-TDSE library, http://code.google.com/p/quantum-sphere-tdse
49. P.J. Kostelec, D.N. Rockmore, SpharmonicKit library, www.cs.dartmouth.edu/geelong/sphere/
50. R. Kosloff, H. Tal-Ezer, Chem. Phys. Lett. **127**, 223 (1986)